Topological Guided Detection of Extreme Wind Phenomena: Implications for Wind Energy

Preprint

Yu Qin,[1,2] Graham Johnson,[2] and Brian Summa[1]

1 Tulane University
2 National Renewable Energy Laboratory

Presented at IEEE VIS and EnergyVis 2023
Melbourne, Australia
October 22-27, 2023

NREL is a national laboratory of the U.S. Department of Energy
Office of Energy Efficiency & Renewable Energy
Operated by the Alliance for Sustainable Energy, LLC

This report is available at no cost from the National Renewable Energy Laboratory (NREL) at www.nrel.gov/publications.

Contract No. DE-AC36-08GO28308

Conference Paper
NREL/CP-2C00-87355
October 2023

Topological Guided Detection of Extreme Wind Phenomena: Implications for Wind Energy

Preprint

Yu Qin,[1,2] Graham Johnson,[2] and Brian Summa[1]

1 Tulane University
2 National Renewable Energy Laboratory

Suggested Citation
Qin, Yu, Graham Johnson, and Brian Summa. 2023. *Topological Guided Detection of Extreme Wind Phenomena: Implications for Wind Energy: Preprint*. Golden, CO: National Renewable Energy Laboratory. NREL/CP-2C00-87355.
https://www.nrel.gov/docs/fy24osti/87355.pdf.

NREL is a national laboratory of the U.S. Department of Energy
Office of Energy Efficiency & Renewable Energy
Operated by the Alliance for Sustainable Energy, LLC

This report is available at no cost from the National Renewable Energy Laboratory (NREL) at www.nrel.gov/publications.

Contract No. DE-AC36-08GO28308

Conference Paper
NREL/CP-2C00-87355
October 2023

National Renewable Energy Laboratory
15013 Denver West Parkway
Golden, CO 80401
303-275-3000 • www.nrel.gov

NOTICE

This work was authored in part by the National Renewable Energy Laboratory, operated by Alliance for Sustainable Energy, LLC, for the U.S. Department of Energy (DOE) under Contract No. DE-AC36-08GO28308. This work was supported by DOE ASCR DE-SC0022873 and NSF IIS 2136744, NIH R01GM143789. The views expressed herein do not necessarily represent the views of the DOE or the U.S. Government. The U.S. Government retains and the publisher, by accepting the article for publication, acknowledges that the U.S. Government retains a nonexclusive, paid-up, irrevocable, worldwide license to publish or reproduce the published form of this work, or allow others to do so, for U.S. Government purposes.

Cover Photos by Dennis Schroeder: (clockwise, left to right) NREL 51934, NREL 45897, NREL 42160, NREL 45891, NREL 48097, NREL 46526.

Topological Guided Detection of Extreme Wind Phenomena: Implications for Wind Energy

Yu Qin
Tulane University — NREL
yu.qin@nrel.gov

Graham Johnson
National Renewable Energy Laboratory (NREL)
graham.johnson@nrel.gov

Brian Summa
Tulane University
bsumma@tulane.edu

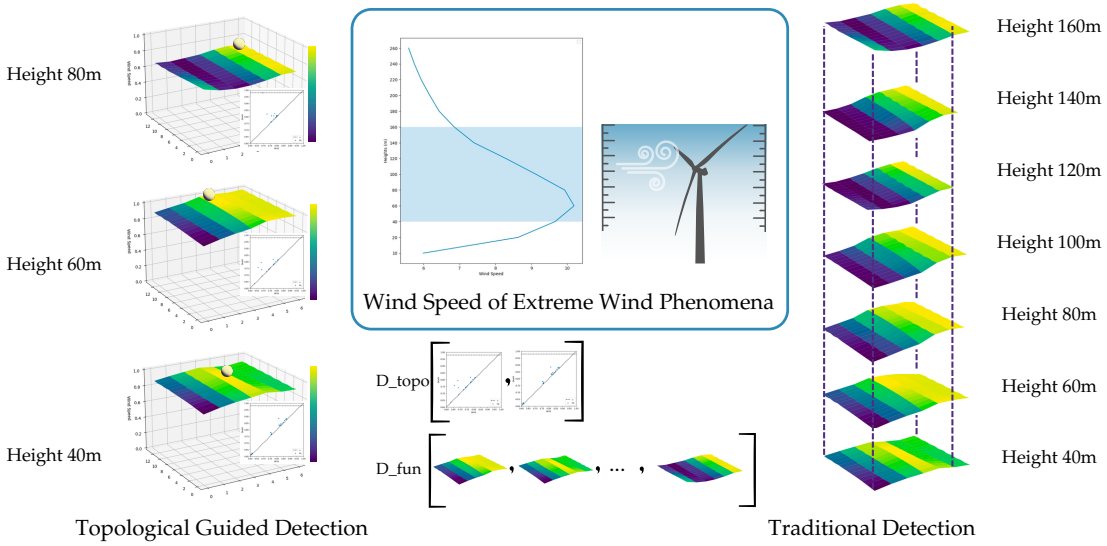

Figure 1: Comparing Topological Guided Detection with Traditional Detection methods, the top middle plot displays a wind speed profile from 10 to 260 meters, highlighting the relevant range for phenomenon occurrence. A distinct curve depicts the category of extreme phenomena impacting wind turbine operations. The left plot presents the sampled regional wind speed profile at three heights alongside its corresponding topological representation. The right plot showcases regional wind speed profiles across all region of interest heights for extreme wind phenomena. The bottom middle plot illustrates the distance function for our method (D_{topo}) and the traditional approach (D_{fun}). Notably, our method requires computation of only a few distances, effectively capturing significant wind speed changes over a broad regional scale. Unlike traditional detection, it eliminates the need for cross-height wind profile comparisons.

Abstract

Extreme wind phenomena play a crucial role in the efficient operation of wind farms for renewable energy generation. However, existing detection methods are computationally expensive, limited to specific coordinate. In real-world scenarios, understanding the occurrence of these phenomena over a large area is essential. Therefore, there is a significant demand for a fast and accurate approach to forecast such events. In this paper, we propose a novel method for detecting wind phenomena using topological analysis, leveraging the gradient of wind speed or critical points in a topological framework. By extracting topological features from the wind speed profile within a defined region, we employ topological distance to identify extreme wind phenomena. Our results demonstrate the effectiveness of utilizing topological features derived from regional wind speed profiles. We validate our approach using high-resolution simulations with the Weather Research and Forecasting model (WRF) over a month in the US East Coast.

Index Terms: Topological Data Analysis—Situational Awareness—Visual Analytics—Wind Energy

1 Introduction

The United States Department of Energy (DOE) has established a target of achieving 30 GW of installed offshore wind capacity by 2030, an amount sufficient to power approximately 10 million homes across the country [13]. Meanwhile, the U.S. East coast currently harbors sixteen active commercial wind energy sites, each in various stages of development [4]. Gaining a better understanding of extreme wind phenomena, specifically Low-Level Jets (LLJs), is of paramount importance for the efficient operation and strategic planning of wind energy systems. LLJs are characterized by strong and persistent winds occurring within a few hundred meters above the Earth's surface. These wind features can possess speeds significantly higher than those found in the surrounding atmospheric layers, making them an essential factor to consider in wind farm management and design [3, 5, 11].

Understanding extreme wind phenomena, such as LLJs, is crucial due to their impact on wind energy usage, turbine structural integrity, and noise levels. Accurate detection and prediction of LLJs allows for optimized operational planning, increased energy production, and mitigating risks associated with mechanical stress and noise emissions. Given the significance of LLJs and their impact on wind energy operations, there is a growing need for accurate detection, prediction, and understanding of these extreme wind phenomena. Advanced methodologies and computational techniques that enable

efficient identification and forecasting of LLJs in large-scale areas are essential for optimizing wind farm performance, ensuring turbine structural integrity, and minimizing potential community impacts. Extensive research efforts are underway to characterize the frequency, intensity, and regimes of low-level jets (LLJs) over the United States using the Weather Research and Forecasting (WRF) model [3, 5, 14, 18, 27, 37]. However, this focus primarily lies in analyzing the behavior of LLJs across different regions and time periods, rather than studying the specific detection methods for LLJs.

Recently, Topological Data Analysis (TDA) has emerged as an effective method for comprehending wind flow [8, 28]. TDA [12], is a powerful tool for extracting and summarizing structural information from complex datasets and has proven its efficacy in providing crucial abstractions of data structures across various fields [6, 7, 15, 16, 22–24, 34, 35]. Topological descriptors such as *persistence diagrams* (PDs) play a crucial role in data analysis and machine learning [1, 19, 22, 31], allowing insights into the structural information of the data and uncover significant features that might be overlooked by other techniques.

While topological-guided visualization has been extensively studied in various fields in a literature review [36], a research gap remains in its application to wind phenomenon detection—a crucial aspect of renewable energy wind farm operation. This paper focuses on investigating TDA's relevance in wind energy. We undertake a comprehensive exploration of TDA for detecting extreme wind phenomena, utilizing the generation of a topological representation of regional wind profiles and calculating their topological distances. The outcome of our investigations demonstrate that, in contrast to existing approaches, TDA offers a systematic and reliable means of comparing wind profiles across different heights and timestamps. This research represents an important initial step towards applying TDA in the analysis of wind phenomena for wind energy systems optimization.

2 Background

2.1 WRF Model

The Weather Research and Forecasting model (WRF) is an advanced numerical weather prediction system extensively utilized in the wind energy community. It plays a crucial role in quantifying wind resources, generating short-term forecasts, and examining meteorological characteristics at the mesoscale and boundary-layer scales, which are vital for analyzing wind speed profiles and wind farm wake effects [9, 17, 29, 33].

The WRF model utilized in this study was initialized using the European Centre for Medium Range Weather Forecasts Interim Reanalysis (ERA-Interim) dataset, employing an initial grid spacing of 54 km. To improve spatial resolution, the WRF model incorporated three internal nested domains, successively refining the resolution to 18 km, 6 km, and eventually reaching 2 km. The model was run over multiple years, with output data extracted at 5-minute intervals. At each grid point and time step, the model provides wind speed values at 14 different heights, ranging from 10m to 260m. These wind speed profiles play a crucial role in analyzing wind resources, assessing meteorological features, and evaluating wind farm performance.

2.2 Identification of Extreme Wind Phenomena

We provide an overview of the identification of extreme wind phenomena. For a detailed description, we refer the reader to [11].

The identification algorithm is applied to 30-minute mean wind speed profiles. It detects two types of wind speed profiles: monotonic shear and low-level jet (LLJ) as shown in Figure 2. Both wind speed profiles are defined as a period of high shear that lasts for 30 minutes or longer.

LLJ are relevant to wind energy operation, so we initially focus on their detection. The main characteristic of an LLJ is that the wind

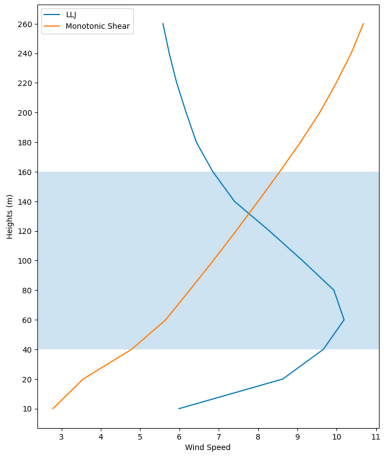

Figure 2: Example of wind profiles at varying heights during two specific time steps simulated by the WRF model along the US East Coast. The blue line represents the low-level jet (LLJ) observed on 5th June 2020, while the orange line corresponds to the monotonic shear on 2nd June 2020. The blue shallow region highlights the specific height range of interest (40m to 160m) where extreme wind phenomena occur. These wind profiles provide valuable insights into the wind behavior during the selected time periods.

speed increases up to a certain height and then decreases. This type of profile is of most interest when it resides within a wind turbine's operational height, which we consider between 40 - 160 meters. We use the following LLJ wind profile identification algorithm:

The gradient of wind speed $\frac{\triangle U}{\triangle z}$ is evaluated, and we first test if it exceeds a predefined threshold value ($0.035s^{-1}$) within the rotor layer (which spans from 40 to 160 m, following [11]).

Next, the height of maximum wind speed is determined, which falls between the second (40 m) and second-to-last (180 m) measurement heights. The wind speed gradient between the bottom of the rotor and the height of the LLJ nose is compared to the same threshold value used for monotonic-shear detection ($0.035s^{-1}$). Additionally, the wind speed drop-off above the LLJ nose must meet the following minimum requirements:

$$\triangle U_{drop} \geqq 1.5ms^{-1}, \frac{\triangle U_{drop}}{U_{nose}} \geqq 10\%,$$

Here, $\triangle U_{drop}$ represents the wind speed difference between U_{top} and U_{nose}, and U_{top} is the first local minimum in the wind speed identified above the nose.

2.3 TDA and distance

Drawing from TDA techniques, we model a dataset as a *filtration*, a sequence of nested topological spaces. Homology and persistent homology are then harnessed for both qualitative and quantitative characterization of these sequences. Homology, involving homology groups and features akin to generators [26], assigns dimensions, like dimension zero for connected components, dimension one for loops, tunnels, and dimension two for voids in $\mathbb{R}^3$. On the other hand, persistent homology measures the homology of the entire filtration [12]. Each feature f_i has a lifespan, with birth time b_i and death time d_i, resulting in a persistence point $(b_i, d_i) \in \mathbb{R}^2$. The persistence diagram represents feature changes through birth-death pairs across the filtration.

In TDA, sublevel set filtration is used to analyze datasets represented by scalar functions, such as wind speed values at different locations in our case. The sublevel set at a specific threshold captures the points in the dataset where the scalar function is less than or equal to that threshold. By varying the threshold, we obtain a

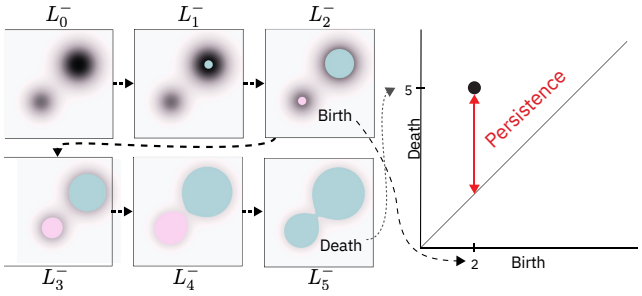

Figure 3: Progression of a sub-level set (L_i^-) of a scalar field for increasing function values (i), where the function values in our case represent wind speed. The green feature emerges at the minimum introduced at 2 and ceases to exist when it merges with a preexisting feature (shown in purple) at 5. The birth and death of the green feature are represented as a point in the 0-dimension persistence diagram, denoted as $(2,5)$. The persistence of this feature is calculated as the difference between its birth and death values (i.e., $5-2=3$).

sequence of nested sublevel sets, providing a hierarchical representation of the dataset and revealing the evolution of topological features. Each feature has a birth time, indicating when it appears, and a death time, indicating when it disappears with other features.

As we increase the threshold value in constructing the sublevel sets, their sizes generally decrease. However, at a certain point, the sublevel set becomes empty, indicating that all points in the dataset have scalar function values greater than the threshold. This empty sublevel set is referred to as the sublevel set at infinity, representing the behavior of the scalar function beyond its maximum value. Figure 3 shows the persistence diagram encodes the topological feature changes that occur throughout the sublevel set filtration process for the scalar field.

The Wasserstein distance measures the dissimilarity between two persistence diagrams by optimizing a matching and summing of the distances between matched points (M) and point-to-diagonal distances for unmatched points (M^c). The one-Wasserstein distance (W1) with $q=1$ is commonly used in applications and is our focus in this work [2, 19]. These diagrams exhibit Lipschitz stability, meaning they are resistant to slight perturbations or noise in the data [10]. This stability allows us to consider diagrams that are close in distance as topologically similar. The Wasserstein distance between persistence diagrams (p1, p2) is defined as:

Wasserstein Distance: Letting $\mathscr{D}$ denote the collection of all diagrams, the q-Wasserstein distance $d_q\colon \mathscr{D}\times\mathscr{D}\to\mathbb{R}$ is defined by

$$d_q(p_1,p_2) := \min_M \left(\sum_{(a,b)\in M} ||a-b||_\infty^q + \frac{1}{2^{q-1}} \sum_{a\in M^c} |a_x - a_y|^q \right)^{1/q},$$

where M ranges over all matchings between persistence diagrams p_1 and p_2, and M^c is the set of persistence points in $p_1 \sqcup p_2$ that do not appear in the matching M; see [10, 20, 21, 25] for more detailed information.

3 Method

In this paper, we propose a topological guided method for the detection of extreme wind phenomena in large-scale regions. Our method consists of three steps: data acquisition, generating topological representations of the wind profile, and calculating the topological distance.

We first acquire wind profile data from the WRF model for a one-month time window in June, as previous studies have indicated that most extreme wind events occur during the summer in our region of interest [4, 11]. We then merge the wind profile data from 5-minute time steps into 30-minute intervals using the mean wind speed, since the extreme wind phenomena lasting for at least 30 minutes are considered relevant for wind farm operation [11]. The region of interest for the wind profile is sampled based on recent research highlighting the significance of the US East Coast [5], which is projected to contribute nearly 3% of the national electricity demand [3].

Data Sampling: The wind speed data we analyzed is in the form of spatial-temporal data, covering various heights. Specifically, it encompasses the latitude range of 39.55°N to 40.00°N and the longitude range of 72.00°W to 73.43°W. This area is represented by a grid composed of 98 units, ensuring extensive data coverage. The analysis period spans from June 1st, 2020 to June 30th, 2020. Wind speeds were measured at different heights, ranging from 10 meters to 260 meters above the ground. This height range is crucial for capturing the vertical variations in wind speed. Moreover, measurements were taken at 20-meter intervals, guaranteeing a detailed depiction of wind patterns across these heights. This concise overview establishes the geographical, temporal, and measurement parameters that provide the context for subsequent data analysis and outcomes.

To achieve accurate detection of extreme wind phenomena at this large scale, we first utilize the sub-level set filtration function to extract the topological representation of the regional wind profile. We use the 0-dimensional topological features in our experiments, which correspond to changes in wind profile for critical point across the entire region. As illustrated in Figure 3, the topological representation is a persistence diagram, where the coordinates (x, y) indicate the birth and death of each topological feature.

In our proposed method, since we use the presistence diagrams to represent the wind profiles, thus, we compare their similarity using the topological distance between persistence diagrams to detect the extreme wind phenomena, instead of directly comparing wind profiles at different heights. We use Wasserstein distance, to compare the similarity between persistence diagrams, the details on how to calculate this distance are explained in Section 2.

To evaluate the effectiveness of our proposed method, we conduct a direct comparison of wind profiles at different heights, which is the typical functional distance. Specifically, we calculate the Euclidean distance for the regional wind profiles at these different heights.

Experiment Details: The wind profile data used in this study was obtained from the WRF model. The data encompasses various parameters, including wind speed, direction, and other relevant measurements, collected from a one-month time window in June 2020 over the US East Coast. To ensure the reliability and accuracy of the data, pre-processing and quality control procedures were applied. Missing or erroneous data points were carefully addressed or removed to maintain the integrity of the dataset. The final dataset consisted of 1,440 30-minute wind profiles.

All experiments were run using the Eagle HPC environment, which is a high-performance computing cluster at NREL. The NREL Wind Toolkit was used to process the wind profile data. The wind profile data is from WRF model. The distance calculation was performed using MPI parallel computation, which allowed the experiments to be run efficiently on the Eagle cluster.

We used Gitto-tda for sub-level set filtration function. This function creates a topological representation of the wind profile by identifying the connected components of the wind speed field. The 0-dimensional topological features have been used in our test, which correspond to the birth and death of connected components in the wind speed field. The infinity death time was removed from the persistence diagrams, as it is not as informative as the features with defined birth and death times.

4 Result

In this section, we demonstrate LLJ detection results for the chosen region and time using the algorithm from [11]. We present identi-

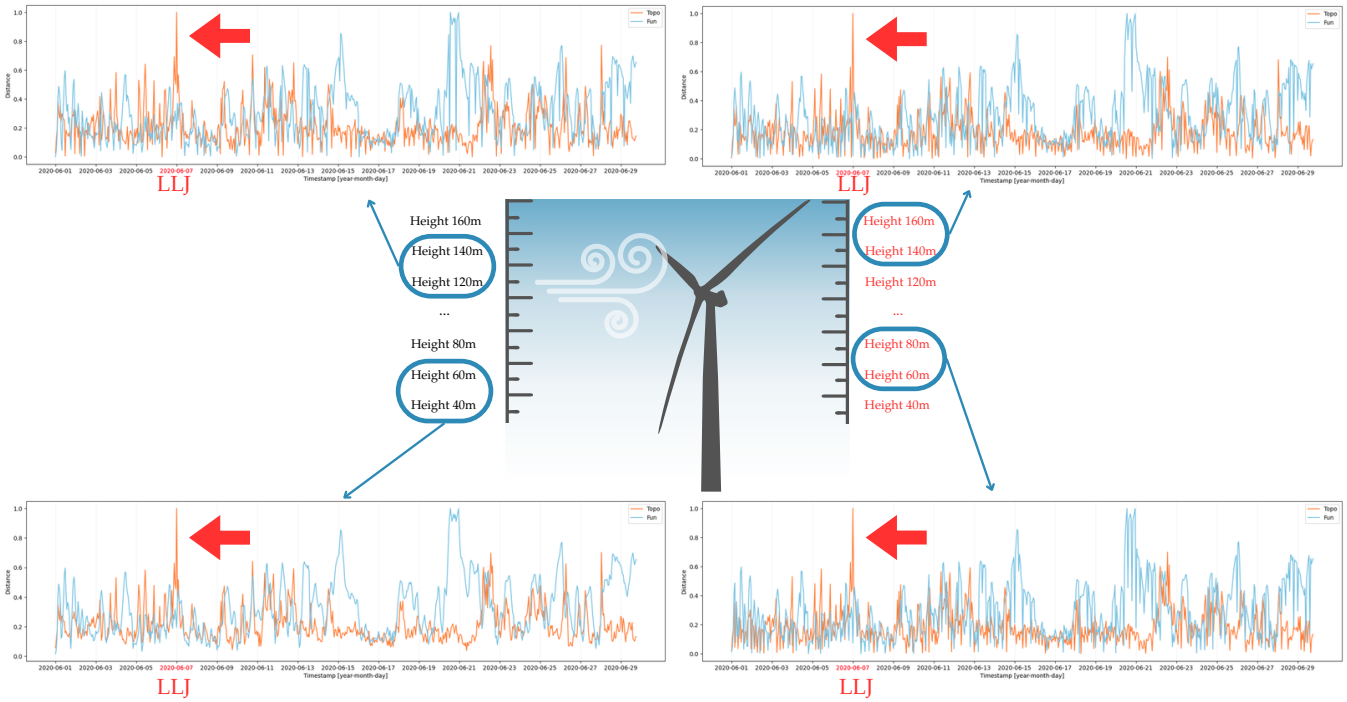

Figure 4: Comparison of Distance Results. The orange line denotes the topological distance derived from the regional wind speed's topological representation, while the blue line represents the functional distance of the regional wind speed. Both distances are computed for two adjacent heights, as indicated by the blue circle points. Red timestamps in each plot highlight extreme wind phenomena. All heights remain within the range defined by the lowest and highest height criteria for extreme wind events. Notably, across various heights, our proposed detection method consistently identifies the LLJ event, as indicated by the red arrow.

fied LLJs for comparison and evaluation. Furthermore, we create the topological representation of the region, facilitating calculation of topological and functional distances at different heights. This analysis assesses the efficacy of our proposed method in detecting extreme wind phenomena.

Figure 2 illustrates wind profiles at different time steps across all heights. Within the one-month window in June, a LLJ event occurred on 5th June 2020, observed in a single cell located at coordinates 39.97° N, 72.72° W. Based on this result, we expanded the grid size to 98 cells using the previous coordinates.

Within the expanded grid, we generated the corresponding topological representation for each cell at each time step and height, followed by the calculation of its topological distance. Comparing the topological distances to the functional distances between the entire grid directly, Figure 4 demonstrates that topological distance can successfully detect extreme wind phenomena even with wind profiles from two different heights while the functional distance cannot. Furthermore, the topological distance consistently produces stable detection results with wind profiles at different heights. These findings support our hypothesis that the topological representation is more effective in encoding critical wind speed information than the traditional functional distance method.

In summary, both topological and functional distances compute the similarity of wind profiles. The topological distance captures topological relationships between wind profile cells, while the functional distance relies on their functional relationships. Our findings reveal the topological distance's superiority in detecting extreme wind phenomena due to its ability to capture distinctive long-range wind speed patterns characteristic of such events.

5 Discussion

The proposed topological guided detection method provides a preliminary result demonstrating its promising applications in wind energy. While this work has been tested on a single dataset, its fast and accurate nature enables timely detection of extreme wind phenomena over large areas, thus optimizing wind farm operations and planning. The efficiency of the method can be further enhanced through fast topology distance comparison [30]. Further research is required to validate the effectiveness and generalizability of this approach across diverse datasets and regions. Moreover, integrating the method with super-resolution generative adversarial network (GAN) models [32] has the potential to improve wind flow simulations by replacing or supplementing computationally expensive WRF models.

Our subsequent task involves mapping the persistence diagram onto the original wind scale field, facilitating the visualization of these extreme phenomena. Such visualization aids wind researchers in conducting faster and more intuitive analyses, enhancing their ability to detect wind phenomena effectively. Additionally, the method's efficiency paves the way for the development of visual analytics systems in wind energy, facilitating real-time analysis and visualization of wind events to enhance decision-making in wind farm operations.

6 Conclusion

Extreme wind phenomena like LLJ events hold significant importance in wind energy due to their distinct attributes, including concentrated high-speed winds and vertical wind shear. These characteristics notably enhance energy production potential and turbine performance. Our study supports the hypothesis that the topological representation outperforms traditional methods in encoding LLJ events, owed to its capability to capture the characteristic long-range wind speed patterns. This approach has the potential to advance LLJ detection accuracy and deepen comprehension of factors driving extreme wind phenomena. The optimization of turbine blade positioning and usage contributes to heightened energy capture and overall turbine efficiency.

ACKNOWLEDGMENTS

This work was authored by the National Renewable Energy Laboratory, managed and operated by Alliance for Sustainable Energy, LLC for the U.S. Department of Energy (DOE) under Contract No. DE-AC36-08G028308. This work was supported by DOE ASCR DE-SC0022873 and NSF IIS 2136744, NIH R01GM143789. The research was performed using computational resources sponsored by the Department of Energy's (DOE) Office of Energy Efficiency and Renewable Energy (EERE) located at the National Renewable Energy Laboratory, and used resources at the Energy Systems Integration Facility, which is a DOE EERE User Facility. The views expressed do not necessarily represent the views of the DOE or the U.S. Government. The U.S. Government retains and the publisher, by accepting the article for publication, acknowledges that the U.S. Government retains a nonexclusive, paid-up, irrevocable, worldwide license to publish or reproduce the published form of this work, or allow others to do so, for U.S. Government purposes.

REFERENCES

[1] *A Stable Multi-Scale Kernel for Topological Machine Learning*, 2015.

[2] H. Adams, T. Emerson, M. Kirby, R. Neville, C. Peterson, P. Shipman, S. Chepushtanova, E. Hanson, F. Motta, and L. Ziegelmeier. Persistence images: A stable vector representation of persistent homology. *Journal of Machine Learning Research*, 18, 2017.

[3] J. A. Aird, R. J. Barthelmie, T. J. Shepherd, and S. C. Pryor. Occurrence of low-level jets over the eastern us coastal zone at heights relevant to wind energy. *Energies*, 15(2):445, 2022.

[4] R. J. Barthelmie, K. E. Dantuono, E. J. Renner, F. L. Letson, and S. C. Pryor. Extreme wind and waves in us east coast offshore wind energy lease areas. *Energies*, 14(4):1053, 2021.

[5] R. J. Barthelmie, T. J. Shepherd, J. A. Aird, and S. C. Pryor. Power and wind shear implications of large wind turbine scenarios in the us central plains. *Energies*, 13(16):4269, 2020.

[6] H. Bhatia, A. G. Gyulassy, V. Lordi, J. E. Pask, V. Pascucci, and P.-T. Bremer. Topoms: Comprehensive topological exploration for molecular and condensed-matter systems. *Journal of Computational Chemistry*, 39(16):936–952, 2018.

[7] P.-T. Bremer, G. Weber, J. Tierny, V. Pascucci, M. Day, and J. Bell. Interactive exploration and analysis of large-scale simulations using topology-based data segmentation. *IEEE Transactions on Visualization and Computer Graphics*, 17(9):1307–1324, 2010.

[8] T. Bridel-Bertomeu, B. Fovet, J. Tierny, and F. Vivodtzev. Topological analysis of high velocity turbulent flow. In *2019 IEEE 9th Symposium on Large Data Analysis and Visualization (LDAV)*, pp. 87–88. IEEE, 2019.

[9] W. Y. Cheng, Y. Liu, A. J. Bourgeois, Y. Wu, and S. E. Haupt. Short-term wind forecast of a data assimilation/weather forecasting system with wind turbine anemometer measurement assimilation. *Renewable Energy*, 107:340–351, 2017.

[10] D. Cohen-Steiner, H. Edelsbrunner, J. Harer, and Y. Mileyko. Lipschitz functions have L_p-stable persistence. *Foundations of Computational Mathematics*, 10(2):127–139, 2010.

[11] M. Debnath, P. Doubrawa, M. Optis, P. Hawbecker, and N. Bodini. Extreme wind shear events in us offshore wind energy areas and the role of induced stratification. *Wind Energy Science*, 6(4):1043–1059, 2021.

[12] H. Edelsbrunner and J. Harer. *Computational Topology: An Introduction*. American Mathematical Soc., 2010.

[13] Energy.gov. Energy secretary granholm announces ambitious new 30gw offshore wind deployment target by 2030, 2021.

[14] S. N. Gadde and R. J. Stevens. Interaction between low-level jets and wind farms in a stable atmospheric boundary layer. *Physical review fluids*, 6(1):014603, 2021.

[15] D. Günther, R. A. Boto, J. Contreras-Garcia, J.-P. Piquemal, and J. Tierny. Characterizing molecular interactions in chemical systems. *IEEE Transactions on Visualization and Computer Graphics*, 20(12):2476–2485, 2014.

[16] A. Gyulassy, P.-T. Bremer, R. Grout, H. Kolla, J. Chen, and V. Pascucci. Stability of dissipation elements: A case study in combustion. *Computer Graphics Forum*, 33(3):51–60, 2014.

[17] A. N. Hahmann, C. L. Vincent, A. Peña, J. Lange, and C. B. Hasager. Wind climate estimation using wrf model output: method and model sensitivities over the sea. *International Journal of Climatology*, 35(12):3422–3439, 2015.

[18] G. Jiménez-Sánchez, P. M. Markowski, V. Jewtoukoff, G. S. Young, and D. J. Stensrud. The orinoco low-level jet: An investigation of its characteristics and evolution using the wrf model. *Journal of Geophysical Research: Atmospheres*, 124(20):10696–10711, 2019.

[19] JMLR. org. *Sliced Wasserstein Kernel for Persistence Diagrams*, 2017.

[20] L. V. Kantorovich. On the translocation of masses. *Journal of Mathematical Sciences*, 133(4):1381–1382, 2006.

[21] M. Kerber, D. Morozov, and A. Nigmetov. Geometry helps to compare persistence diagrams. *Journal of Experimental Algorithmics (JEA)*, 22:1–20, 2017.

[22] P. Lawson, A. B. Sholl, J. Q. Brown, B. T. Fasy, and C. Wenk. Persistent homology for the quantitative evaluation of architectural features in prostate cancer histology. *Scientific Reports*, 9(1):1–15, 2019.

[23] D. Maljovec, B. Wang, P. Rosen, A. Alfonsi, G. Pastore, C. Rabiti, and V. Pascucci. Topology-inspired partition-based sensitivity analysis and visualization of nuclear simulations. *Proc. of IEEE PacificVis*, 2016.

[24] Z. Meng, D. V. Anand, Y. Lu, J. Wu, and K. Xia. Weighted persistent homology for biomolecular data analysis. *Scientific Reports*, 10(1):1–15, 2020.

[25] G. Monge. Mémoire sur la théorie des déblais et des remblais. *Histoire de l'Académie Royale des Sciences de Paris*, 1781.

[26] J. R. Munkres. *Algebraic Topology*. Prentice Hall, Upper Saddle River, NJ, 1964.

[27] C. G. Nunalee and S. Basu. Mesoscale modeling of coastal low-level jets: implications for offshore wind resource estimation. *Wind Energy*, 17(8):1199–1216, 2014.

[28] D. Ofori-Boateng, H. Lee, K. M. Gorski, M. J. Garay, and Y. R. Gel. Application of topological data analysis to multi-resolution matching of aerosol optical depth maps. *Frontiers in Environmental Science*, 9:684716, 2021.

[29] S. C. Pryor, T. J. Shepherd, P. J. Volker, A. N. Hahmann, and R. J. Barthelmie. "wind theft" from onshore wind turbine arrays: sensitivity to wind farm parameterization and resolution. *Journal of Applied Meteorology and Climatology*, 59(1):153–174, 2020.

[30] Y. Qin, B. T. Fasy, C. Wenk, and B. Summa. A domain-oblivious approach for learning concise representations of filtered topological spaces for clustering. *IEEE Transactions on Visualization and Computer Graphics*, 28(1):302–312, 2021.

[31] Springer. *Topological Machine Learning with Persistence Indicator Functions*, 2017.

[32] K. Stengel, A. Glaws, D. Hettinger, and R. N. King. Adversarial super-resolution of climatological wind and solar data. *Proceedings of the National Academy of Sciences*, 117(29):16805–16815, 2020.

[33] B. Storm and S. Basu. The wrf model forecast-derived low-levelwind shear climatology over the united states great plains. *Energies*, 3(2):258–276, 2010.

[34] Wiley Online Library. *Stable topological signatures for points on 3d shapes*, vol. 34, 2015.

[35] K. Xia and G.-W. Wei. Persistent homology analysis of protein structure, flexibility, and folding. *International journal for numerical methods in biomedical engineering*, 30(8):814–844, 2014.

[36] L. Yan, T. B. Masood, R. Sridharamurthy, F. Rasheed, V. Natarajan, I. Hotz, and B. Wang. Scalar field comparison with topological descriptors: Properties and applications for scientific visualization. *Computer Graphics Forum*, 40(3):599–633, 2021. doi: 10.1111/cgf.14331

[37] M. Zhang and Z. Meng. Warm-sector heavy rainfall in southern china and its wrf simulation evaluation: A low-level-jet perspective. *Monthly Weather Review*, 147(12):4461–4480, 2019.